

Calibration and cancellation of microwave crosstalk in superconducting circuits

Haisheng Yan(严海生), Shoukuan Zhao(赵寿宽), Zhongcheng Xiang(相忠诚), Ziting Wang(王子婷), Zhaohua Yang(杨钊华), Kai Xu(许凯), Ye Tian(田野), Haifeng Yu(于海峰), Dongning Zheng(郑东宁), Heng Fan(范桁), and Shiping Zhao(赵士平)

Citation: Chin. Phys. B, 2023, 32 (**9**): 094203. DOI: 10.1088/1674-1056/acdc10
Journal homepage: http://cpb.iphy.ac.cn; http://iopscience.iop.org/cpb

What follows is a list of articles you may be interested in

Realization of adiabatic and diabatic CZ gates in superconducting qubits coupled with a tunable coupler

Huikai Xu(徐晖凯), Weiyang Liu(刘伟洋), Zhiyuan Li(李志远), Jiaxiu Han(韩佳秀), Jingning Zhang(张静宁), Kehuan Linghu(令狐克寰), Yongchao Li(李永超), Mo Chen(陈墨), Zhen Yang(杨真), Junhua Wang(王骏华), Teng Ma(马腾), Guangming Xue(薛光明), Yirong Jin(金贻荣), and Haifeng Yu(于海峰)

Chin. Phys. B, 2021, 30 (**4**): 044212. DOI: 10.1088/1674-1056/abf03a

Phase-sensitive Landau-Zener-Stückelberg interference in superconducting quantum circuit

Zhi-Xuan Yang(杨智璇), Yi-Meng Zhang(张一萌), Yu-Xuan Zhou(周宇轩), Li-Bo Zhang(张礼博), Fei Yan(燕飞), Song Liu(刘松), Yuan Xu(徐源), and Jian Li(李剑)

Chin. Phys. B, 2021, 30 (**2**): 024212. DOI: 10.1088/1674-1056/abd753

Cavity-induced ATS effect on a superconducting Xmon qubit

Xueyi Guo(郭学仪), Hui Deng(邓辉), Jianghao Ding(丁江浩), Hekang Li(李贺康), Pengtao Song(宋鹏涛), Zhan Wang(王战), Luhong Su(苏鹭红), Yanjun Liu(刘彦军), Zhongcheng Xiang(相忠诚), Jie Li(李洁), Yirong Jin(金贻荣), Yuxi Liu(刘玉玺), Dongning Zheng(郑东宁)

Chin. Phys. B, 2018, 27 (**8**): 084202. DOI: 10.1088/1674-1056/27/8/084202

Quantum state transfer via a hybrid solid-optomechanical interface

Pei Pei(裴培), He-Fei Huang(黄鹤飞), Yan-Qing Guo(郭彦青), Xing-Yuan Zhang(张兴远), Jia-Feng Dai(戴佳峰)

Chin. Phys. B, 2018, 27 (**2**): 024203. DOI: 10.1088/1674-1056/27/2/024203

Fabrication and characterization of ultra-low noise narrow and wide band Josephson parametric amplifiers

Keqiang Huang(黄克强), Qiujiang Guo(郭秋江), Chao Song(宋超), Yarui Zheng(郑亚锐), Hui Deng(邓辉), Yulin Wu(吴玉林), Yirong Jin(金贻荣), Xiaobo Zhu(朱晓波), Dongning Zheng(郑东宁)

Chin. Phys. B, 2017, 26 (**9**): 094203. DOI: 10.1088/1674-1056/26/9/094203

Calibration and cancellation of microwave crosstalk in superconducting circuits

Haisheng Yan(严海生)[1,2], Shoukuan Zhao(赵寿宽)[3], Zhongcheng Xiang(相忠诚)[1], Ziting Wang(王子婷)[1,2], Zhaohua Yang(杨钊华)[1,2], Kai Xu(许凯)[1,2,4,†], Ye Tian(田野)[1], Haifeng Yu(于海峰)[3,4], Dongning Zheng(郑东宁)[1,2,4,5,6], Heng Fan(范桁)[1,2,4,5,6], and Shiping Zhao(赵士平)[1,2,4,5,6]

[1] *Beijing National Laboratory for Condensed Matter Physics, Institute of Physics, Chinese Academy of Sciences (CAS), Beijing* 100190, *China*
[2] *School of Physical Sciences, University of Chinese Academy of Sciences (UCAS), Beijing* 100190, *China*
[3] *Beijing Academy of Quantum Information Sciences, Beijing* 100193, *China*
[4] *Hefei National Laboratory, Hefei* 230088, *China*
[5] *CAS Center for Excellence in Topological Quantum Computation, UCAS, Beijing* 100190, *China*
[6] *Songshan Lake Materials Laboratory, Dongguan* 523808, *China*

(Received 6 April 2023; revised manuscript received 31 May 2023; accepted manuscript online 7 June 2023)

The precise control and manipulation of the qubit state are vital for quantum simulation and quantum computation. In superconducting circuits, one notorious error comes from the crosstalk of microwave signals applied to different qubit control lines. In this work, we present a method for the calibration and cancellation of the microwave crosstalk and experimentally demonstrate its effectiveness in a superconducting 10-qubit chain. The method is convenient and efficient especially for calibrating the microwave crosstalk with large amplitudes and variations, which can be performed successively to reduce the microwave crosstalk by two to three orders. The qubit chain with microwave driving is governed by one-dimensional (1D) Bose–Hubbard model in transverse field, which is nonintegrable and shows thermalization behaviour during the time evolution from certain initial states. Such thermalization process is observed with excellent agreement between experiment and theory further confirming the effective global cancellation of the microwave crosstalk.

Keywords: superconducting qubit, microwave crosstalk, Rabi oscillation

PACS: 42.50.Dv, 03.67.Lx, 05.30.Jp, 85.25.Cp **DOI:** 10.1088/1674-1056/acdc10

1. Introduction

Superconducting qubits are an excellent platform for quantum simulation and quantum computation,[1–3] which have been widely used to simulate many-body phenomena in condensed-matter physics[4–13] and demonstrate quantum advantage.[14,15] In the applications, the precise controls of qubits are required and crosstalks among different control lines need to be eliminated. Qubit controls usually utilize flux bias signals for tuning the energy level spacing (Z control) and microwave signals for manipulating the quantum state (XY control). With the present-day devices fabricated by the flip-chip technology etc., crosstalk among the Z control lines can be made as small as 0.1%.[13] However, crosstalk among the XY control lines remains relatively large, usually above 1%. Further eliminating the crosstalk of the XY control lines, or the microwave crosstalk, is therefore important for the applications of superconducting circuits.

The microwave crosstalk signal can be eliminated in principle by cancellation with a compensation signal of the same amplitude and frequency but 180° out-of-phase. This method is used in quantum simulation experiments of dynamical phase transitions[7] and thermalization,[8] in which all superconducting qubits are biased with the same frequency. More recently, it is also applied to the superconducting circuits with different fixed-frequency qubits, using the alternative-current Stark effect to measure the Stark-induced phase for the determination of the compensation signal parameters.[16] The microwave crosstalk effect and its mitigation have also been investigated to improve the gate performance.[17,18]

In this work, we present and experimentally demonstrate a method of calibrating and cancelling the microwave crosstalk via compensation signals, in which systematic formulation and steps for obtaining the crosstalk matrix are described. Our method can be applied to superconducting circuits with frequency-tunable qubits operating with a common frequency as well as different frequencies. The crosstalk matrix can be conveniently determined for a given device with orders of magnitude difference of crosstalk strengths among different qubit control lines. We will use a superconducting 10-qubit chain device (see Fig. 1) with the crosstalk strength ranging from 0.18% to 98%, (The crosstalk strength has wide variation for the present device, which partly results from the specific sample design. For instance, the XY control lines of Q_1 and Q_{10} locate at different qubit positions compared to those of Q_2 through Q_9. Also, the XY control lines of Q_2 to Q_6 sit at the opposite side of the Z control lines as compared to the cases of Q_7 to Q_9 (see Fig. 1).) and demonstrate the successful calibration and cancellation of microwave crosstalk by two to three orders. The qubit chain is governed by 1D Bose–Hubbard model, which is nearly integrable when the high level

†Corresponding author. E-mail: kaixu@iphy.ac.cn

© 2023 Chinese Physical Society and IOP Publishing Ltd

states are only sparsely populated.[12,19] The model becomes nonintegrable when a microwave field is applied.[8,19,20] We will show a clear thermalization process in the nonintegrable system, demonstrating that the microwave crosstalk is globally suppressed.

2. Microwave crosstalk in superconducting circuits

To start, we present a general formulation for quantifying the microwave crosstalk in a superconducting circuit of N qubits with different frequencies. We define $\Omega_m(t)$ and $\Omega'_m(t)$ as the actual microwave signal which a qubit receives and the driving signal input to the XY control line of this qubit, respectively, as shown in Fig. 2 in the simple case with two qubits. To determine the crosstalk matrix, one applies microwave signals to the control lines and measure the responses of the qubits. Therefore $\Omega'_m(t)$ does not contain cross-qubit terms and we write

$$\begin{aligned}\Omega_m(t) &= \Omega_{mm}\cos(\omega_m t+\varphi_{mm}) \\ &\quad+\sum_{n=1(n\neq m)}^{N}\Omega_{mn}\cos(\omega_n t+\varphi_{mn}+\varphi_{nn}),\\ \Omega'_m(t) &= \Omega_{mm}\cos(\omega_m t+\varphi_{mm}).\end{aligned}\tag{1}$$

Here Ω_{mn} and φ_{mn} are the parameters for signals applied on the mth qubit by the nth qubit drive with frequency ω_n, thus those with $n\neq m$ describe the microwave crosstalk signals. For the matrix representation, it is convenient to rewrite Eq. (1) in the form with complex quantities:

$$\begin{aligned}\Omega_m(t) &= \Omega_{mm}\,\mathrm{e}^{\mathrm{i}(\omega_m t+\varphi_{mm})} \\ &\quad+\sum_{n=1(n\neq m)}^{N}\Omega_{mn}\,\mathrm{e}^{\mathrm{i}(\omega_n t+\varphi_{mn}+\varphi_{nn})},\\ \Omega'_m(t) &= \Omega_{mm}\,\mathrm{e}^{\mathrm{i}(\omega_m t+\varphi_{mm})}.\end{aligned}\tag{2}$$

It is clear that taking the real part of Eq. (2) goes back to Eq. (1). We further define column vectors $\boldsymbol{\Omega}(t)$ and $\boldsymbol{\Omega}'(t)$ as

$$\boldsymbol{\Omega}(t)=(\Omega_1(t),\Omega_2(t),\ \ldots,\ \Omega_N(t))^{\mathrm{T}},\tag{3a}$$

$$\boldsymbol{\Omega}'(t)=(\Omega'_1(t),\Omega'_2(t),\ \ldots,\ \Omega'_N(t))^{\mathrm{T}}\tag{3b}$$

to have

$$\boldsymbol{\Omega}(t)=\boldsymbol{M}\boldsymbol{\Omega}'(t),\tag{4}$$

in which $\boldsymbol{M}$ is the crosstalk matrix defined by

$$\boldsymbol{M}=\begin{pmatrix}1 & a_{12}\,\mathrm{e}^{\mathrm{i}\varphi_{12}} & \ldots & a_{1N}\,\mathrm{e}^{\mathrm{i}\varphi_{1N}}\\ a_{21}\,\mathrm{e}^{\mathrm{i}\varphi_{21}} & 1 & \ldots & a_{2N}\,\mathrm{e}^{\mathrm{i}\varphi_{2N}}\\ \vdots & \vdots & \ddots & \vdots\\ a_{N1}\,\mathrm{e}^{\mathrm{i}\varphi_{N1}} & a_{N2}\,\mathrm{e}^{\mathrm{i}\varphi_{N2}} & \ldots & 1\end{pmatrix}\tag{5}$$

with $a_{mn}=\Omega_{mn}/\Omega_{nn}$. We will show how to determine the matrix $\boldsymbol{M}$ below. With known $\boldsymbol{M}$, the required microwave signals input from the qubit drive lines can be calculated for the given signals actually applied on qubits for performing a specific operation in the circuit, via

$$\boldsymbol{\Omega}'(t)=\boldsymbol{M}^{-1}\boldsymbol{\Omega}(t).\tag{6}$$

Here $\boldsymbol{M}^{-1}$ is the inverse matrix of $\boldsymbol{M}$. We note that after obtaining $\boldsymbol{M}$, in contrast to the definitions in Eqs. (1) and (2), an $\boldsymbol{\Omega}(t)$ without cross-qubit terms is often required for specific operations in experiment. On the other hand, $\boldsymbol{\Omega}'(t)$ applied to the qubit control lines calculated from Eq. (6) will contain all terms, namely signals with different frequencies need to be applied to a given qubit control line in order to cancel the crosstalk signals from the other qubit control lines.

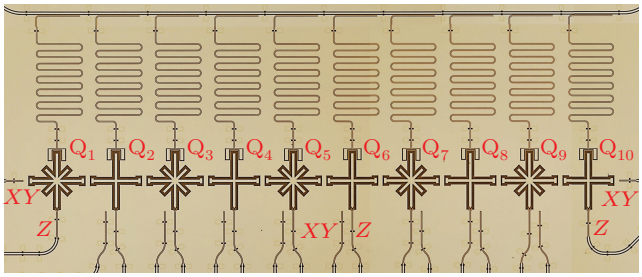


Fig. 1. Optical micrograph of the superconducting 10-qubit chain. Each qubit has a microwave line for XY control, a flux bias line for Z control, and a readout resonator for measurement.

The physical meaning of the parameters in the above formulation can be readily seen. In the two-qubit case shown in Fig. 2, the microwave signals are experimentally applied to the drive lines of qubits Q_1 and Q_2, which, according to Eq. (1), are $\Omega'_1(t)=\Omega_{11}\cos(\omega_1 t+\varphi_{11})$ and $\Omega'_2(t)=\Omega_{22}\cos(\omega_2 t+\varphi_{22})$, respectively. Writing these in the form of Eq. (2), inserting them into Eq. (4), and taking the real parts, we have for Q_1:

$$\Omega_1(t)=\Omega_{11}\cos(\omega_1 t+\varphi_{11})+\Omega_{12}\cos(\omega_2 t+\varphi_{12}+\varphi_{22}),\tag{7}$$

which is also given by Eq. (1). Here Ω_{mn} are the Rabi frequencies of the m-th qubit by the n-th qubit drive with frequency ω_n. Since the matrix $\boldsymbol{M}$ has unity diagonal elements, equation (4) says that the line attenuations are taken into account by first experimentally calibrating Ω_{11} and Ω_{22} for corresponding signal strength (or amplitude) applied to the control lines. Ω_{12} and φ_{12} in Eq. (7) can be obtained in the following way. We first set $\omega_1=\omega_2$ and $\varphi_{22}=0$. Q_1 is also biased to ω_2 while Q_2 is biased far away (e.g., 200 MHz or above) to be decoupled from Q_1. We have

$$\Omega_1(t)=\Omega_{11}\cos(\omega_2 t+\varphi_{11})+\Omega_{12}\cos(\omega_2 t+\varphi_{12}).\tag{8}$$

With these the Hamiltonian of Q_1 reads

$$\hat{H}_1=\frac{1}{2}\omega_{\mathrm{q}}\sigma^z+\Omega_1(t)\sigma^x.\tag{9}$$

Using the rotation wave approximation we have

$$\begin{aligned}\hat{H}_1 &= \frac{1}{2}\Delta_{\mathrm{q}}\sigma^z+\frac{1}{2}(\Omega_{11}\,\mathrm{e}^{\mathrm{i}\varphi_{11}}+\Omega_{12}\,\mathrm{e}^{\mathrm{i}\varphi_{12}})\sigma^+\\ &\quad+\frac{1}{2}(\Omega_{11}\,\mathrm{e}^{-\mathrm{i}\varphi_{11}}+\Omega_{12}\,\mathrm{e}^{-\mathrm{i}\varphi_{12}})\sigma^-,\end{aligned}\tag{10}$$

in which $\Delta_q = \omega_q - \omega_2$ is the qubit detuning with respect to the driving frequency, usually set to zero in experiment. The Rabi frequency Ω_R of Q_1 is found to be

$$\Omega_R = \sqrt{\Delta_q^2 + \Omega_{11}^2 + \Omega_{12}^2 + 2\Omega_{11}\Omega_{12}\cos(\varphi_{12} - \varphi_{11})}. \quad (11)$$

We will show experimentally that with given Ω_{11}, Ω_{22}, $\omega_1 = \omega_2$, and $\varphi_{22} = 0$, one can measure the Rabi frequency Ω_R of Q_1 as a function of φ_{11}, and the parameters Ω_{12} and φ_{12} can be obtained by fitting the experimental data using Eq. (11). The corresponding matrix element in M is therefore determined. Note that when $\varphi_{11} = \varphi_{12}$, Ω_R reaches a maximum value, indicating that the signals arriving at Q_1 from the two drive lines have a common phase. In other words, $\varphi_{12} \pm 2\pi n$ represents the phase difference resulting from the different delay times across the two drive lines.

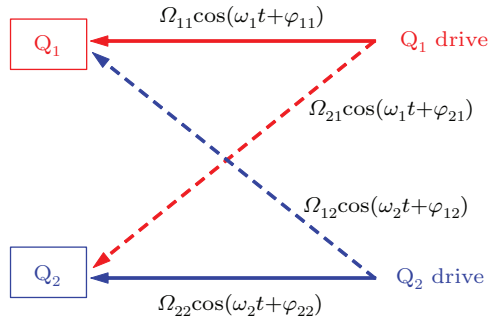


Fig. 2. Schematic diagram of microwave signal crosstalk shown with two qubits as an example. Here Ω_{mn} and φ_{mn} are the parameters for signals applied on the m-th qubit by the n-th qubit drive with frequency ω_n.

To measure the Rabi frequency, we note that the rotation axis $\boldsymbol{n}$ of the Rabi oscillation in Bloch sphere is

$$\boldsymbol{n} = (n_x, n_y, n_z) \quad (12a)$$

with

$$n_x = \frac{1}{\Omega_R}\left[\Omega_{11}\cos\varphi_{11} + \Omega_{12}\cos\varphi_{12}\right], \quad (12b)$$

$$n_y = \frac{1}{\Omega_R}\left[\Omega_{11}\sin\varphi_{11} + \Omega_{12}\sin\varphi_{12}\right], \quad (12c)$$

$$n_z = \frac{\Delta_q}{\Omega_R}. \quad (12d)$$

The unitary operator for the state evolution becomes

$$\hat{U}(t) = \mathrm{e}^{-\mathrm{i}\Omega_R t(\boldsymbol{n}\cdot\boldsymbol{\sigma})/2}, \quad (13)$$

where $\boldsymbol{\sigma}$ is the Pauli matrices. For Q_1 initialized in the ground state $|0\rangle$, its time evolution is

$$|\psi\rangle = U(t)|0\rangle \quad (14)$$

and the probability P_1 that Q_1 stays in the first-excited state $|1\rangle$ is given by

$$P_1 = \langle\psi|1\rangle\langle 1|\psi\rangle = \sin^2\frac{\Omega_R t}{2}(n_x^2 + n_y^2). \quad (15)$$

The Rabi frequency Ω_R can be obtained by measuring P_1 versus time t. For Q_2, the parameters Ω_{21} and φ_{21} can be known in the similar way, and all the matrix elements in M are then determined by the measurements between different qubit pairs.

The above formulation of the microwave crosstalk considering different superconducting qubit frequencies should be useful for multiqubit systems where qubit frequencies are much crowded so that certain qubit frequencies are not possible to set sufficiently apart for precise gate operations.[16,18] However, without loss of generality, we will experimentally demonstrate our method for the calibration and cancellation of microwave crosstalk in the superconducting 10-qubit chain with widely varied crosstalk strength in the resonant case, namely with all qubits biased at the same frequency, a situation in which numerous analog quantum simulation experiments are performed.[5–13] A photograph of the device used in the experiment is shown in Fig. 1 and its basic parameters are listed in Table 1.

Table 1. Basic device parameters. f_m and f_i are the qubit maximum and idle frequencies. U_j is the qubit anharmonicity. T_1 and T_2^* are the energy relaxation and dephasing times of the qubit at idle point. $J_{j,j+1}$ and $J_{j,j+2}$ are the coupling strengths of nearest neighbor (NN) and next nearest neighbor (NNN) qubits. The working frequency ω_0 is 4.445 GHz.

	Q_1	Q_2	Q_3	Q_4	Q_5	Q_6	Q_7	Q_8	Q_9	Q_{10}
f_m (GHz)	5.308	5.896	5.387	5.097	5.144	5.395	5.327	5.804	5.389	5.726
f_i (GHz)	4.221	5.265	4.381	5.048	4.278	5.234	4.418	5.023	4.297	5.158
$U_j/2\pi$ (MHz)	–212	–264	–210	–268	–212	–268	–214	–264	–214	–264
T_1 (μs)	47.6	26.3	40.4	17.5	23	29.3	46	30.8	38.2	29.3
T_2^* (μs)	1.97	2.34	1.74	6.36	2.12	5.64	2.63	3.79	3.51	1.54
$J_{j,j+1}/2\pi$ (MHz)		10.72	10.73	10.99	11.05	10.88	10.48	10.86	10.79	10.78
$J_{j,j+2}/2\pi$ (MHz)		0.98	0.49	0.96	0.49	0.96	0.49	0.97	0.48	

3. Experimental results and discussion

Quantum simulation experiments of thermalization in nonintegrable systems are usually performed using the quench process with an initial state evolving under suddenly changed Hamiltonian and all qubits set at a common working frequency ω_0. We will use $\omega_0/2\pi = 4.445$ GHz for the simulation experiment to test the global elimination of microwave crosstalk. To demonstrate our crosstalk calibration method, we consider

Q_1 and Q_2, and determine the parameters Ω_{12} and φ_{12}. For this, we set $\Delta_q = 0$, $\omega_1 = \omega_2 = \omega_0$, $\Omega_{11}/2\pi = 10$ MHz, $\Omega_{22}/2\pi = 58$ MHz, and $\varphi_{22} = 0$. Here Ω_{22} needs to be larger than Ω_{11} to observe a clear crosstalk effect. We then measure the time evolution of P_1 as a function of φ_{11}. The results are shown in Fig. 3(a) with the extracted Rabi frequency versus φ_{11} plotted in panel (b) with symbols (further improved results are shown in Fig. 4, as discussed below). Fitting the experimental data in Fig. 3(b) with Eq. (11), shown as a solid line, we obtain $\Omega_{12}/2\pi = 56.97$ MHz and $\varphi_{12} = 1.8377$, leading to $a_{12} = 98.22\%$. Here φ_{12} is equal to φ_{11} with maximum Rabi frequency, as can be seen in Eq. (11). Likewise for the measurement of Ω_{21} and φ_{21}, we set $\Omega_{11}/2\pi = 58$ MHz, $\Omega_{22}/2\pi = 10$ MHz, and $\varphi_{11} = 0$, and measure the time evolution of P_1 as a function of φ_{22}. Repeating the above procedure, we obtain $\Omega_{21}/2\pi = 4.095$ MHz and $\varphi_{21} = -1.808$, leading to $a_{21} = 7.06\%$.

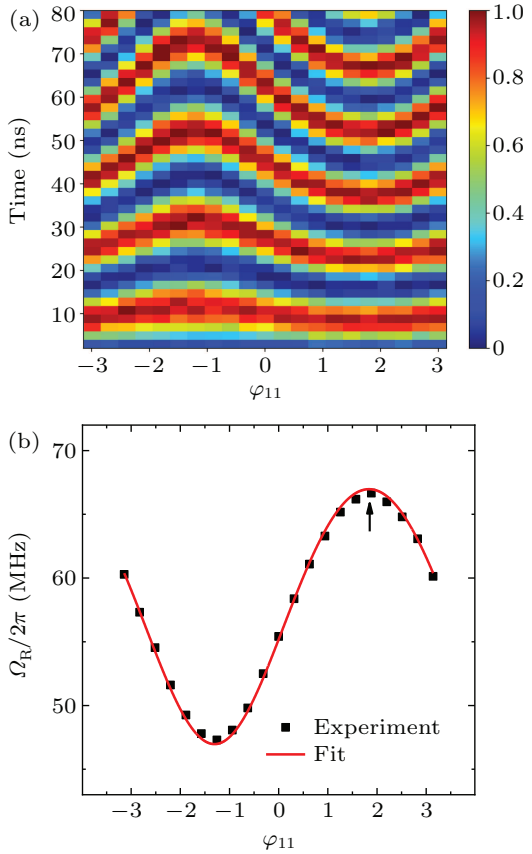


Fig. 3. (a) Experimental time dependence of P_1 as a function of φ_{11} for Q_1 at the first stage for the measurement of M_1. $\Omega_{11}/2\pi = 10$ MHz, $\Omega_{22}/2\pi = 58$ MHz, and $\varphi_{22} = 0$ are used for the microwave signals input to the qubit control lines. (b) Rabi frequency versus φ_{11} extracted from the data in panel (a) (symbols). The solid line is a fit with Eq. (11), from which we obtain $\Omega_{12}/2\pi = 56.97$ MHz and $\varphi_{12} = 1.8377$, giving rise to $a_{12} = 98.22\%$. An upward arrow indicates the point where $\varphi_{12} = \varphi_{11}$ with maximum Rabi frequency.

The obtained crosstalk matrix elements between Q_1 and Q_2 are illustrated in Fig. 5(a). We see that the matrix element a_{12} is nearly 100%, meaning that when we apply a microwave signal to Q_2, a signal of nearly the same amplitude will also be applied to Q_1. Unlike the superconducting device with all-to-all qubit connection,[7] a strongly varied crosstalk strength is expected for the present chain-like device due to the special sample configuration. For such device, multiple crosstalk calibration and cancellation steps are required. In practice, with known $\boldsymbol{M}$ we can use Eq. (6) to calculate the microwave signals $\boldsymbol{\Omega}'(t)$ that need to be applied to the control lines for the actual signals $\boldsymbol{\Omega}(t)$ required on the qubits. To test how accurately the calibration can be achieved, we consider Q_1 and Q_2 and experimentally set $\boldsymbol{\Omega}'(t)$ with $\Omega_{11}/2\pi = 10$ MHz, $\Omega_{22}/2\pi = 58$ MHz, $\varphi_{22} = 0$, and check Rabi oscillations of Q_1 versus φ_{11} again. However, these signals are transformed by $\boldsymbol{M}^{-1}$ before applied to the qubit control lines (note that $\boldsymbol{M}$ is a 2×2 matrix at the moment). Let us use $\boldsymbol{M}_1$ to denote $\boldsymbol{M}$ obtained above. Due to the experimental errors of various kinds and large crosstalk near 100% and quantum crosstalk resulting from ZZ interaction[21,22] in the system, $\boldsymbol{M}_1$ may not accurately describe the microwave crosstalk of the system. If a matrix $\boldsymbol{M} = \boldsymbol{M}_2\boldsymbol{M}_1$ better describes the microwave crosstalk, we have $\boldsymbol{\Omega}(t) = \boldsymbol{M}_2\boldsymbol{M}_1\boldsymbol{\Omega}'(t)$. The transformation by $\boldsymbol{M}_1^{-1}$ means experimentally setting $\boldsymbol{\Omega}'(t) \to \boldsymbol{M}_1^{-1}\boldsymbol{\Omega}'(t)$, and we have $\boldsymbol{\Omega}(t) = \boldsymbol{M}_2\boldsymbol{\Omega}'(t)$. The matrix $\boldsymbol{M}_2$ in this case is expected to be close to a unit matrix with off-diagonal elements close to zero.

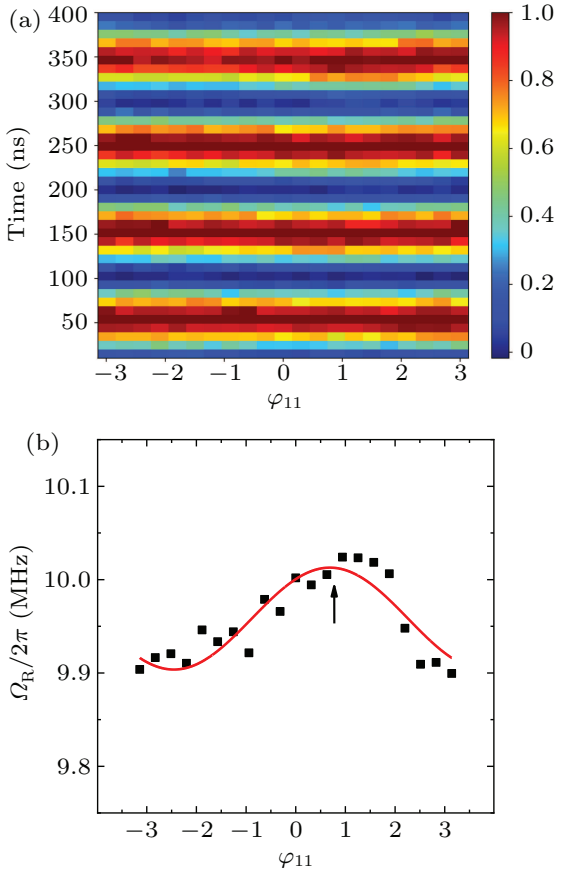


Fig. 4. (a) Experimental time dependence of P_1 as a function of φ_{11} for Q_1 at the fourth stage for the measurement of M_4. $\Omega_{11}/2\pi = 10$ MHz, $\Omega_{22}/2\pi = 58$ MHz, and $\varphi_{22} = 0$ are used for the microwave signals input to the qubit control lines. (b) Rabi frequency versus φ_{11} extracted from the data in panel (a) (symbols). The solid line is a fit with Eq. (11), from which we obtain $\Omega_{12}/2\pi = 0.0573$ MHz and $\varphi_{12} = 0.6876$, giving rise to $a_{12} = 0.099\%$. An upward arrow indicates the point where $\varphi_{12} = \varphi_{11}$ with maximum Rabi frequency.

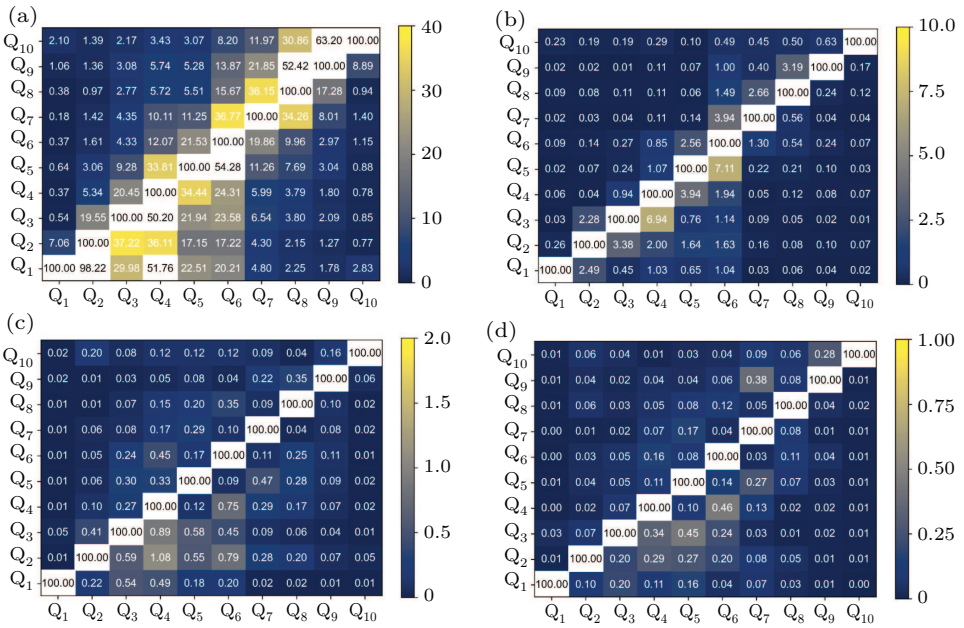


Fig. 5. Microwave crosstalk calibration matrices of (a) $\boldsymbol{M}_1$, (b) $\boldsymbol{M}_2$, (c) $\boldsymbol{M}_3$, and (d) $\boldsymbol{M}_4$ obtained at four successive stages, in which the color bars represent the matrix element values up to 40%, 10%, 2%, and 1%, respectively. The data above these values are illustrated in black and white. The average values of off-diagonal matrix elements for $\boldsymbol{M}_1$, $\boldsymbol{M}_2$, $\boldsymbol{M}_3$, and $\boldsymbol{M}_4$ are 13.50%, 0.7415%, 0.1823%, and 0.0808%, respectively.

The similar measurements of Rabi oscillations of Q_1 versus φ_{11} and of Q_2 versus φ_{22} result in the parameters of $\Omega_{12}/2\pi = 1.443$ MHz, $\varphi_{12} = 1.706$, $\Omega_{21}/2\pi = 0.1494$ MHz, and $\varphi_{21} = 1.130$ for $\boldsymbol{M}_2$, giving rise to $a_{12} = 2.49\%$ and $a_{21} = 0.26\%$, which are illustrated in Fig. 5(b). $\boldsymbol{M}_2$ obtained at this second stage provides a proper estimate of how precise $\boldsymbol{M}_1$ calibrates the microwave crosstalk of the system. Similarly, we can write $\boldsymbol{M} = \cdots \boldsymbol{M}_i \cdots \boldsymbol{M}_1$ with $\boldsymbol{M}_i$ closer to unit matrix for larger i. Figures 5(c) and 5(d) illustrate the results for $\boldsymbol{M}_3$ and $\boldsymbol{M}_4$, respectively. At each calibration stage, $\boldsymbol{M} = \cdots \boldsymbol{M}_i \cdots \boldsymbol{M}_1$ is calculated in the 10×10 matrix form (see below) and the 2×2 matrices are taken from the results to obtain the 2×2 inverse matrices for input signal transformation. Experimental results of Rabi oscillations of Q_1 corresponding to the data in Fig. 3 and producing the matrix elements of $\boldsymbol{M}_4$ at the fourth stage are presented in Fig. 4. We can see a much smaller variation amplitude of the Rabi oscillation with φ_{11} due to a much reduced Ω_{12} [see Eq. (11)], which leads to a much reduced a_{12}.

The above microwave crosstalk calibration method used between Q_1 and Q_2 are applied to other qubit pairs in the 10-qubit chain. The results of $\boldsymbol{M}_1$ through $\boldsymbol{M}_4$ are presented in Fig. 5. It can be seen that at the second calibration stage, namely with $\boldsymbol{M} = \boldsymbol{M}_2\boldsymbol{M}_1$, the crosstalk among the qubits are already well below 1%, which can be seen and estimated from $\boldsymbol{M}_3$ in Fig. 5. The average values of off-diagonal matrix elements for $\boldsymbol{M}_1$, $\boldsymbol{M}_2$, $\boldsymbol{M}_3$, and $\boldsymbol{M}_4$ are 13.50%, 0.7415%, 0.1823%, and 0.0808%, respectively.

To further test the effectiveness of the calibration, we consider the 10-qubit chain driven by a continuous microwave field. In the rotating frame with a common qubit frequency, the system is governed by the 1D Bose–Hubbard model in a transverse field[4,6,20] reads

$$H = H' + H'' + \sum_{j=1}^{10} \frac{U_j}{2} n_j(n_j - 1) + \sum_{j=1}^{10} \frac{\Omega}{2}(a_j^\dagger + a_j), \qquad (16)$$

in which $H' = \sum_{j=1}^{9} J_{j,j+1}(a_j^\dagger a_{j+1} + \text{h.c.})$ and $H'' = \sum_{j=1}^{8} J_{j,j+2}(a_j^\dagger a_{j+2} + \text{h.c.})$ are the hopping terms with nearest and next-nearest neighbor coupling strengths $J_{j,j+1}$ and $J_{j,j+2}$, respectively. The third term on the right-hand side is the on-site interaction with anharmonicity $U_j \leq 0$. $a_j^\dagger$ (a_j) is the bosonic creation (annihilation) operator and $n_j = a_j^\dagger a_j$ is the number operator. The last term in Eq. (16) is the transverse field with constant strength Ω from the microwave driving written in the rotating frame of the driving frequency resonant with the qubit common frequency.[20]

Equation (16) well describes the 10-qubit chain driven under a continuous microwave field. The sample parameters U_j, $J_{j,j+1}$, and $J_{j,j+2}$ are listed in Table 1. In Fig. 6, we show the experimental (symbols) and calculated (lines) time evolutions of the local observables $\langle\sigma^z\rangle_0 = (1/5)\sum_{\text{odd}\,j}\langle\sigma_j^z\rangle$ and $\langle\sigma^z\rangle_1 = (1/5)\sum_{\text{even}\,j}\langle\sigma_j^z\rangle$ starting from the Néel initial state $|0101010101\rangle$ (lines).[20] Here $\langle\sigma_j^z\rangle$ is the expectation value of σ_j^z of j-th qubit. Experimentally, the Néel state is prepared with the qubits biased at their respective idle frequencies listed in Table 1 via the Z control lines. Then the microwave field is applied via the XY control lines with the qubits set at the common frequency ω_0 for state evolution and the observables σ_j^z is measured for each qubit at different evolving times. Figure 6(a) shows the results for $\Omega/2\pi = 0$, with which the system is near integrable. The expected fluctuating behaviour of the observables during the evolution can be clearly seen with

good agreement between experiment and theory. The calculated results with $\Omega/2\pi = 5$ MHz, where the system becomes nonintegrable, are plotted as lines in Figs. 6(b) and 6(c). Both $\langle\sigma^z\rangle_0$ and $\langle\sigma^z\rangle_1$ exhibit a fast thermalization behaviour,[8,19,20] quickly decreasing and increasing to zero from $+1$ and -1, respectively. Experimental results in Fig. 6(b) are measured without microwave calibration showing clear deviations between experiment and theory, while those in Fig. 6(c) with the calibration using $\boldsymbol{M} = \boldsymbol{M}_3\boldsymbol{M}_2\boldsymbol{M}_1$ crosstalk matrix (see Fig. 5 for $\boldsymbol{M}_1$, $\boldsymbol{M}_2$, and $\boldsymbol{M}_3$). Excellent agreements between the experimental and theoretical data Fig. 6(c) confirm the effectiveness and accuracy of our crosstalk calibration and cancellation method.

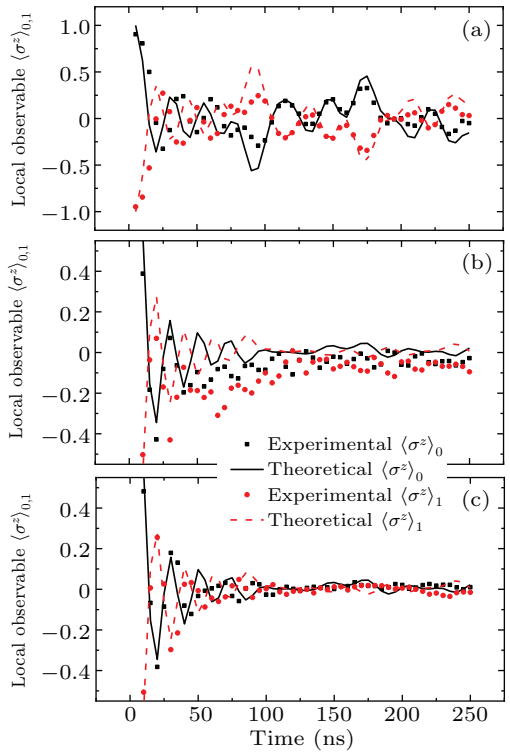


Fig. 6. Time evolutions of local observables $\langle\sigma^z\rangle_0 = (1/5)\sum_{\text{odd}\,j}\langle\sigma_j^z\rangle$ and $\langle\sigma^z\rangle_1 = (1/5)\sum_{\text{even}\,j}\langle\sigma_j^z\rangle$ from the Néel initial state $|0101010101\rangle$ under the Hamiltonian Eq. (16). (a) $\Omega/2\pi = 0$ MHz, showing a fluctuating behaviour of the observables in near integrable system. (b) $\Omega/2\pi = 5$ MHz, suggesting thermalization of nonintegrable system in microwave field without calibration. (c) $\Omega/2\pi = 5$ MHz, demonstrating a fast thermalization process of nonintegrable system in calibrated microwave field, with good agreement between experiment and theory.

In the previous experiment,[7] the crosstalk matrix elements are measured in two steps. Let us consider Q_1 and Q_2 again. Also after the calibrations of Ω_{11} and Ω_{22}, Ω_{12} is first determined by setting $\Omega_{11} = 0$ and applying Ω_{22} with $\varphi_{22} = 0$. In the second step, $\Omega_{11} = \Omega_{12}$ is used. Then φ_{12} is found by measuring the Rabi frequency against φ_{22} with $\varphi_{11} = 0$. The present experiment combines the two steps into one. Since we have set $\Omega_{11}/2\pi = 10$ MHz in the calibration, from Eq. (11) we always have the Rabi frequency above 10 MHz, corresponding to an oscillation period below 100 ns, which is convenient for the measurement. In practice, we find the present method convenient and efficient especially for calibrating and cancelling the microwave crosstalk with large amplitudes and wide variations such as those in the 10-qubit chain device. Using repeated measurements of $\boldsymbol{M}_i$ in $\boldsymbol{M} = \cdots\boldsymbol{M}_i\cdots\boldsymbol{M}_1$, we can successively improve the accuracy of the calibration and cancellation of the microwave crosstalk.

As a final remark, we emphasize that our method for the microwave crosstalk calibration can be applied to the case with different qubit frequencies though the calibrations discussed so far are performed with a common qubit frequency for the quantum quench experiment. In the cases with different qubit frequencies, the calibration for each qubit pair can be done in exactly the same way. Generally, the amplitude and phase of the crosstalk matrix elements are frequency-dependent, as can be seen in Fig. 7 for Q_1 and Q_2 measured in the frequency range between 4.445 GHz and 4.695 GHz. Therefore, the crosstalk calibration of a given qubit pair needs to be done again when their working frequencies change.

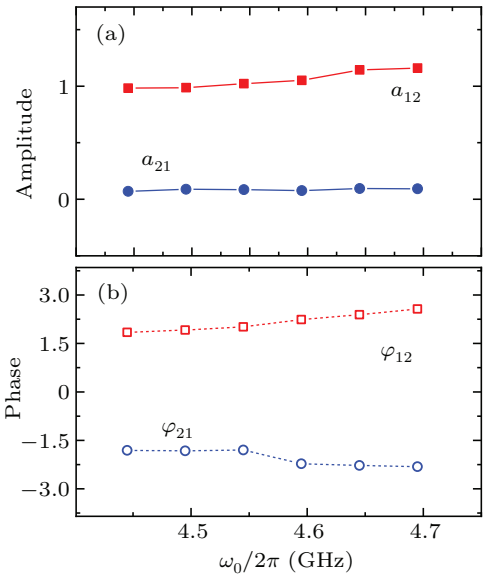


Fig. 7. Measured frequency dependences of the amplitude (a) and phase (b) of the microwave crosstalk matrix elements for Q_1 and Q_2.

4. Summary

We have presented a method for the calibration and cancellation of microwave crosstalk in superconducting circuits. Starting from a general formulation of the problem, in which the crosstalk matrix was defined and the matrix elements could be found from the qubit Rabi oscillations, we proceeded to experimentally demonstrate the calibration and cancellation of microwave crosstalk and its effectiveness in a superconducting 10-qubit chain. We showed that a matrix element could be determined in a single step by measuring the Rabi frequency of a given qubit as a function of the phase of the signal applied to this qubit control line, while another signal was applied to the control line of the crosstalking qubit. We found that the method was convenient and efficient especially for calibrating

and cancelling the microwave crosstalk with large amplitudes and extensive variations like those in the 10-qubit chain device studied in this work. The calibration and cancellation could be performed successively to reduce the microwave crosstalk effectively by two to three orders. We further tested the method by the observation of the thermalization phenomena in the nonintegrable system with excellent agreement between experiment and theory.

Acknowledgements

Project supported by the Key-Area Research and Development Program of Guangdong Province, China (Grant No. 2018B030326001) and the National Natural Science Foundation of China (Grant No. 11874063). H F Yu acknowledges supports from the Natural Science Foundation of Beijing (Grant No. Z190012) and the National Natural Science Foundation of China (Grant No. 11890704). H Fan acknowledges supports from the National Natural Science Foundation of China (Grant Nos. 11934018 and T2121001), Strategic Priority Research Program of the Chinese Academy of Sciences (Grant No. XDB28000000), and Beijing Natural Science Foundation (Grant No. Z200009).

References

[1] Krantz P, Kjaergaard M, Yan F, Orlando T P, Gustavsson S and Oliver W D 2019 *Appl. Phys. Rev.* **6** 021318
[2] Altman E, Brown K R, Carleo G, *et al.* 2021 *PRX Quantum* **2** 017003
[3] Daley A J, Bloch I, Kokail C, Flannigan S, Pearson N and Zoller P 2022 *Nature* **607** 667
[4] Roushan P, Neill C, Tangpanitanon J, Bastidas V M, Megrant A, Barends R, Chen Y, Chen Z, Chiaro B, Dunsworth A, Fowler A, Foxen B, Giustina M, Jeffrey E, Kelly J, Lucero E, Mutus J, Neeley M, Quintana C, Sank D, Vainsencher A, Wenner J, White T, Neven H, Angelakis D G and Martinis J 2017 *Science* **358** 1175
[5] Xu K, Chen J J, Zeng Y, Zhang Y R, Song C, Liu W X, Guo Q J, Zhang P F, Xu D, Deng H, Huang K Q, Wang H, Zhu X B, Zheng D N and Fan H 2018 *Phys. Rev. Lett.* **120** 050507
[6] Yan Z, Zhang Y R, Gong M, Wu Y, Zheng Y, Li S, Wang C, Liang F, Lin J, Xu Y, Guo C, Sun L, Peng C Z, Xia K, Deng H, Rong H, You J Q, Nori F, Fan H, Zhu X and Pan J W 2019 *Science* **364** 753
[7] Xu K, Sun Z H, Liu W X, Zhang Y R, Li H K, Dong H, Ren W H, Zhang P F, Nori F, Zheng D N, Fan H and Wang H 2020 *Sci. Adv.* **6 (25)** eaba4935
[8] Chen F, Sun Z H, Gong M, Zhu Q L, Zhang Y R, Wu Y, Ye Y, Zha C, Li S, Guo S, Qian H, Huang H L, Yu J, Deng H, Rong H, Lin J, Xu Y, Sun L, Guo C, Li N, Liang F, Peng C Z, Fan H, Zhu X B and Pan J W 2021 *Phys. Rev. Lett.* **127** 020602
[9] Braumüller J, Karamlou A H, Yanay Y, Kannan B, Kim D, Kjaergaard M, Melville A, Niedzielski B M, Sung Y, Vepsäläinen A, Winik R, Yoder J L, Orlando T P, Gustavsson S, Tahan C and Oliver W D 2022 *Nat. Phys.* **18** 172
[10] Karamlou A H, Braumüller J, Yanay Y, Paolo A D, Harrington P M, Kannan B, Kim D, Kjaergaard M, Melville A, Muschinske S, Niedzielski B M, Vepsäläinen A, Winik R, Yoder J L, Schwartz M, Tahan C, Orlando T P, Gustavsson, S and Oliver W D 2022 *npj Quantum Inf.* **8** 35
[11] Zhao S K, Ge Z Y, Xiang Z, Xue G M, Yan H S, Wang Z T, Wang Z, Xu H K, Su F F, Yang Z H, Zhang H, Zhang Y R, Guo X Y, Xu K, Tian Y, Yu H F, Zheng D N, Fan H and Zhao S P 2022 *Phys. Rev. Lett.* **129** 160602
[12] Zhu Q, Sun Z H, Gong M, Chen F, Zhang Y R, Wu Y, Ye Y, Zha C, Li S, Guo S, Qian H, Huang H L, Yu J, Deng H, Rong H, Lin J, Xu Y, Sun L, Guo C, Li N, Liang F, Peng C Z, Fan H, Zhu X B and Pan J W 2022 *Phys. Rev. Lett.* **128** 160502
[13] Li X G, Xu H K, Wang J H, Tang L Z, Zhang D W, Yang C H, Su T, Wang C L, Mi Z Y, Sun W J, Liang X H, Chen M, Li C Y, Zhang Y S, Linghu K H, Han J X, Liu W Y, Feng Y L, Liu P, Xue G M, Zhang J N, Jin Y R, Zhu S L, Yu H F and Xue Q K 2023 arXiv: 2301.12138
[14] Arute F, Arya K, Babbush R, *et al.* 2019 *Nature* **574** 505
[15] Wu Y, Bao W S, Cao S, *et al.* 2021 *Phys. Rev. Lett.* **127** 180501
[16] Nuerbolati W, Han Z K, Chu J, Zhou Y X, Tan X S, Yu Y, Liu S and Yan F 2022 *Appl. Phys. Lett.* **120** 174001
[17] Sung Y, Ding L, Braumüller J, Vepsäläinen A, Kannan B, Kjaergaard M, Greene A, Samach G O, McNally C, Kim D, Melville A, Niedzielski B M, Schwartz M E, Yoder J L, Orlando T P, Gustavsson S and Oliver W D 2021 *Phys. Rev. X* **11** 021058
[18] Wang R X, Zhao P and Jin Y R and Yu H F 2022 *Appl. Phys. Lett.* **121** 152602
[19] Yan H S, Wang Y Y, Zhao S K, Yang Z H, Wang Z T, Xu K, Tian Y, Yu H F, Fan H and Zhao S P 2023 arXiv: 2302.05169
[20] Bañuls M C, Cirac J I and Hastings M B 2011 *Phys. Rev. Lett.* ***106*** 050405
[21] Patterson A D, Rahamim J, Tsunoda T, Spring P A, Jebari S, Ratter K, Mergenthaler M, Tancredi G, Vlastakis B, Esposito M and Leek P J 2019 *Phys. Rev. Appl.* **12** 064013
[22] Zhao P, Linghu K H, Li Z Y, Xu P, Wang R, Xue G, Jin Y R and Yu H F 2022 *PRX Quantum* **3** 020301